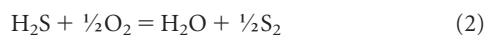# LETTERS

Redox evolution of a degassing magma rising to the surface

Alain Burgisser[1] & Bruno Scaillet[1]

Volatiles carried by magmas, either dissolved or exsolved, have a fundamental effect on a variety of geological phenomena, such as magma dynamics[1–5] and the composition of the Earth's atmosphere[6]. In particular, the redox state of volcanic gases emanating at the Earth's surface is widely believed to mirror that of the magma source, and is thought to have exerted a first-order control on the secular evolution of atmospheric oxygen[6,7]. Oxygen fugacity (f_{O_2}) estimated from lava or related gas chemistry, however, may vary by as much as one log unit[8–10], and the reason for such differences remains obscure. Here we use a coupled chemical–physical model of conduit flow to show that the redox state evolution of an ascending magma, and thus of its coexisting gas phase, is strongly dependent on both the composition and the amount of gas in the reservoir. Magmas with no sulphur show a systematic f_{O_2} increase during ascent, by as much as 2 log units. Magmas with sulphur show also a change of redox state during ascent, but the direction of change depends on the initial f_{O_2} in the reservoir. Our calculations closely reproduce the H_2S/SO_2 ratios of volcanic gases observed at convergent settings, yet the difference between f_{O_2} in the reservoir and that at the exit of the volcanic conduit may be as much as 1.5 log units. Thus, the redox state of erupted magmas is not necessarily a good proxy of the redox state of the gases they emit. Our findings may require re-evaluation of models aimed at quantifying the role of magmatic volatiles in geological processes.

Recent studies have investigated the role of redox equilibria during volatile exsolution, but the solution of the numerical problem requires fixing either iron or sulphur redox states[11]: as a result, the effect of decompression on f_{O_2} cannot be evaluated. In the present work, we relax such an assumption by taking advantage of the fact that the solubility laws of key volatile species other than H_2O and CO_2 have been recently determined, in particular those of H_2, SO_2 and H_2S (refs 12, 13). We consider gas phases in the system H–O–S, with six species (H_2O, H_2, SO_2, H_2S, S_2 and O_2), in which the following redox equilibria occur:

$$H_2 + \tfrac{1}{2}O_2 = H_2O \qquad (1)$$

$$H_2S + \tfrac{1}{2}O_2 = H_2O + \tfrac{1}{2}S_2 \qquad (2)$$

$$O_2 + \tfrac{1}{2}S_2 = SO_2 \qquad (3)$$

Standard thermodynamic considerations[14,15] show that once total pressure (P), temperature (T), and two additional intensive parameters such as water and hydrogen fugacities (f_{H_2O} and f_{H_2}) are known, the fugacities of all remaining species (f_{H_2S}, f_{O_2}, f_{S_2}, f_{SO_2}) are fixed and the gas phase composition in the H–O–S system is fully determined. Each species i in the gas has a mole fraction m_i: $\sum m_i = 1$.

The gas phase is modelled as an ideal mixture of non-ideal gases, a valid approximation in the pressure range considered here. Departure from ideal behaviour of end-member species is accounted for by the fugacity coefficient γ_i, which is fixed by P and T (ref. 16). The total weight fraction of each species (w_{Ti}) is the sum of its exsolved part (w_{gi}) and its dissolved part: $w_{Ti} = w_{gi} + a_i(\gamma_i m_i P)^{b_i}$, where a_i and b_i are experimentally determined solubility constants (Table 1). We use a homogeneous, one-dimensional conduit flow model[5] to simulate magma ascent under closed-system and equilibrium conditions. Magma rises in a cylindrical conduit at constant mass flux, and volatile exsolution affects the flow through changes in buoyancy and viscosity (see Supplementary Information). Calculations are performed by first fixing P, T, f_{H_2O}, f_{H_2} and the amount of gas in the reservoir. The model seeks first the equilibrium distribution of each volatile species between gas and melt before ascent. Then, at each next lower pressure, mass conservation requires that total amounts of each element (O, H and S) remain constant. Using this constraint, the model calculates the equilibrium distribution of volatile species, which in turn affects ascent dynamics.

Redox equilibrium during magma ascent involving dissolved iron can be written as:

$$Fe_2O_3 = 2FeO + \tfrac{1}{2}O_2 \qquad (4)$$
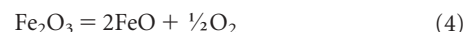
The importance of such a reaction will be dictated by the initial amount of dissolved iron oxides. We have simulated the redox effect of iron by using an empirical model that relates the FeO/Fe_2O_3 ratio of silicate melts to f_{O_2} (ref. 17; here f_{O_2} is referenced to the solid buffer Ni−NiO, such that NNO + 1 means an f_{O_2} one order of magnitude higher than NNO). Runs under typical storage conditions of arc rhyolites ($\leq$1 wt% total iron and f_{O_2} between NNO − 1 and NNO + 1;) show that reaction (4) partly buffers changes in f_{O_2} when little gas is present in the reservoir (<0.2 log units without changing the redox trend during ascent, see Supplementary Information). In contrast, in iron-rich liquids such as basalts, the buffering capacity of iron species will be higher. Thus our results primarily apply to magmas in which the residual melt is rhyolitic, as commonly observed in arc settings. We did not consider the role of iron in crystals because

Table 1 | Solubility constants

Species	a_i	b_i
H_2O	1.063×10^{-3}	0.5399
H_2	3.400×10^{-7}	1.2800
SO_2	1.632×10^{-10}	1.3789
H_2S	8.239×10^{-6}	0.5145
O_2	0	0
S_2	0	0

The parameters a_i and b_i were determined by fitting experimental solubility data of corresponding species to an empirical equation of the form $w_i = a_i f_i^{b_i}$. We have used data from ref. 12 for sulphur-bearing species, from ref. 13 for hydrogen, and from ref. 29 for water.

[1]ISTO, UMR 6113 Université d'Orléans-CNRS, 1a rue de la Férollerie, 45071 Orléans cedex 2, France.

the role of solid buffers as a first-order mechanism controlling redox state during magma ascent can be ruled out on kinetic grounds. The lattice diffusion processes that this mechanism requires are exceedingly slow compared to those in gas or liquid phases.

Similarly, for simplicity we have not investigated the role of CO_2, as detailed petrologic studies of silicic magmas in arcs show them to have little or no CO_2 under pre-eruptive conditions[18]. In general, however, introduction of CO_2 will lower f_{H_2O} and thus drive our calculated values towards lower f_{O_2} via equilibrium (1). Our assumption of equilibrium implies that the model might not capture the chemical evolution of the gas within rapidly decompressed magmas, such as in plinian eruptions, in which the contrasted diffusive kinetics of volatile species may inhibit attainment of equilibrium. Both H_2O and H_2 are, however, fast diffusing species relative to CO_2 and S-bearing ones[18,19]. Thus, if physical fractionation of volatile species arises during ascent, the gas phase composition will be driven towards the system H–O (C and S species remain in the melt, as documented for S for the 1991 Pinatubo eruption[20]), which will exert a dominant control on the redox state of escaping gases. Our model thus represents a fundamental end-member case towards which magmas, notably those andesitic to silicic in arc settings, tend to evolve.

We have explored the following range of starting conditions, typical of silicic arc magmas[21,22]: an initial pressure from 2,000 to 3,000 bar, f_{O_2} from NNO + 2 to NNO − 0.5, bulk iron contents (FeO* = FeO + Fe_2O_3/1.113) up to 3 wt%, bulk water contents up to 10.4 wt% and bulk sulphur contents up to 3 wt%, the last two parameters being adjusted by varying the amount of excess gas in the reservoir (up to 5 wt%; ref. 23). The conduit radius was fixed at 5 m for all runs. Temperature has been fixed to 825 °C, that is, typical of rhyolite magmas[21], and melt density to 2,140 kg m^{-3}, though different choices will not affect the trends observed. Runs are constrained to reach atmospheric pressure at the vent, which yields initial ascent rates between 0.7 and 12 m s^{-1}. Because degassing occurs in equilibrium, changes in chemistry as a function of pressure occur regardless of ascent speed. In all cases, the simulations are carried down to atmospheric pressure, though it can be anticipated that the last increments of f_{O_2} change we compute might not be

reached, owing either to the inhibiting effect of viscosity at low water content[24] or to gas loss once a permeability threshold is reached such that the system becomes open to gas[25].

We first consider the S- and Fe-free case. All simulations performed showed essentially identical behaviour in terms of redox state evolution, that is, the f_{O_2} of the magma increases during ascent, the magnitude of increase being more or less damped by the amount of free gas present in the reservoir. A representative example is shown in Fig. 1, corresponding to a magma initially stored at 2,000 bar, at an f_{O_2} of NNO − 0.2, with a melt H_2O content of 5.46 wt%, and for excess gas contents of 0.1, 1 and 5 wt%. The simulations show that the magnitude of f_{O_2} change increases when the amount of excess gas decreases, and can reach more than 2 log units for a gas-poor magma (0.1 wt%).

We now explore the case of S-bearing rhyolite magma with 1 wt% of total iron and stored at 2,000 bar, illustrating our calculations with three different initial f_{O_2} but similar initial dissolved S contents (~200–250 p.p.m.). A magma starting at an f_{O_2} of NNO − 0.5 displays a continuous increase in its f_{O_2} as it ascends, except in the last few hundred bars where a reversal in f_{O_2} towards reduction occurs (Fig. 2). The magnitude of change is strongly dependent on the amount of gas initially present in the reservoir. At low gas content (0.1 wt%), the f_{O_2} rises by 0.7 log units relative to starting conditions. With 5 wt% gas, the magma has a redox state nearly constant up to a pressure of 100 bar. When the starting f_{O_2} in the reservoir is at NNO (Fig. 2), the magma undergoes oxidation only for gas-poor conditions (0.1 wt%). Higher amounts of gas in the reservoir impart a reducing trend in the f_{O_2} evolution during ascent, the final f_{O_2} differing by almost 1 log unit from the initial value for an initial gas content of 5 wt%. When the initial f_{O_2} in the reservoir is at NNO + 1.5, the magma undergoes a significant reduction during ascent regardless of its initial gas content (Fig. 2). In this case, the drop in f_{O_2} may exceed 1.5 log units at near-atmospheric conditions for gas-rich conditions.

The change in f_{O_2} during decompression is accompanied by dramatic changes in gas phase composition (Fig. 3). Our calculated H_2S/SO_2 ratios fall in the range 0.1–10, which is comparable to that of volcanic gases measured at convergent settings for silicic to intermediate magmas[26] (Fig. 3). Clearly, a variety of H_2S/SO_2 ratios can be
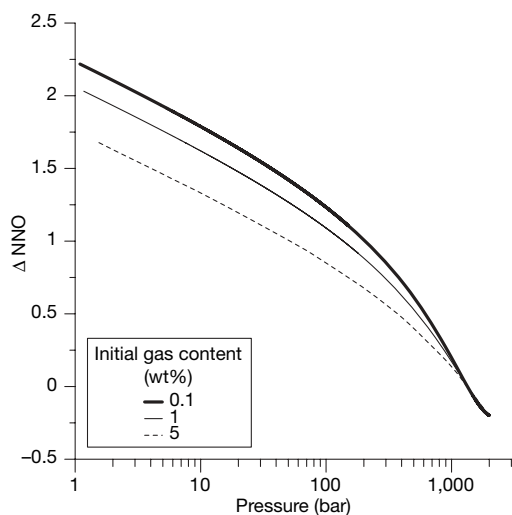

Figure 1 | Fundamental relationship between magma ascent and magma redox state, for a rhyolite magma coexisting with a H–O gas. From gas content and composition at depth, the coupled model of conduit flow calculates the evolution of the physical and chemical conditions of the ascending magma. The effect of equilibrium degassing is a systematic increase in f_{O_2} with decreasing pressure (that is, with shallower depth). Here f_{O_2} is referenced to the solid buffer Ni−NiO (NNO); NNO + 1 means an f_{O_2} one order of magnitude higher than NNO, and is expressed as ΔNNO = 1). The figure shows representative cases, for three initial values of exsolved volatiles with an f_{H_2} initially fixed at 10 bar.
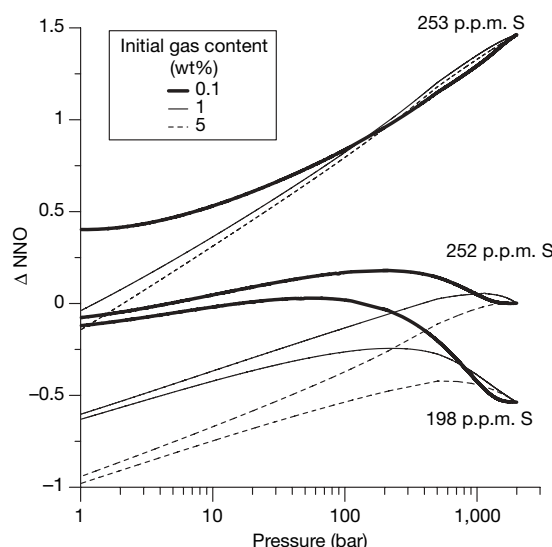

Figure 2 | Fundamental relationship between magma ascent and magma redox state, for a rhyolite magma coexisting with a H–O–S gas. The effect of initial redox state on its evolution during decompression is shown. The graph shows representative cases, for three initial values of exsolved volatiles with an f_{H_2O} initially fixed at 1,000 bar. The initial redox state was achieved by varying f_{H_2} (ΔNNO = −0.5, f_{H_2} = 10; ΔNNO = 0, f_{H_2} = 5.38; ΔNNO = +1.5, f_{H_2} = 1).

produced from magmas having common initial redox states but different amounts of gases. Conversely, a given H_2S/SO_2 ratio may be produced from a wide range of starting redox conditions. For instance, a H_2S/SO_2 ratio of about one can be produced from a magma initially stored at NNO + 1.5 with 5 wt% gas, or from a magma initially at NNO − 0.5 with 0.1 wt% gas (Fig. 3a). Thus, anticipating the H_2S/SO_2 ratio of gases emanating from a given reservoir would require knowing not only the reservoir f_{O_2}, but also the amount of free gas present in the reservoir and the depth at which gas and melt are physically separated. Although such a rich behaviour precludes a simple explanation for each trend calculated, a sensitivity analysis of our model suggests that water exsolution plays an important role in oxidizing the system, and that, on the other hand, the complex pressure dependence of the redox equilibria (1)–(3) contribute to the reducing trends. Our findings have thus obvious implications for the use of volcanic gases as a monitoring tool of volcanic activity. They also illustrate the important role of sulphur. Magmas poor in sulphur or in which reactions involving sulphur are kinetically inhibited are likely to undergo a significant increase in their redox state during ascent.

The above results show that the redox state that magma records at depth does not necessarily mirror that of its escaping gases, in particular when they are released from levels shallower than the main reservoir. Thus, from a broader perspective, our findings have implications for our understanding of how past volcanic activity may have affected Earth's atmosphere. Current models of the evolution of atmospheric oxygen implicitly assume that the redox state of magmatic rocks can be taken as equal to that of their outgassed products[6,7]. Our calculations show that, for silicic magmas, this assumption holds true only under a restricted set of conditions (for instance, a magma starting at NNO − 0.5 with 1 wt% gas, Fig. 2). Oxidized silicic magmas are particularly prone to redox change during ascent. A recent study[10] has stressed the difference in f_{O_2} retrieved from volcanic gas[11] and volcanic glass[12] at Kilauea volcano: the basaltic glass, which is fully degassed, records an f_{O_2} that is 1.2 log units lower than that of the gas. Although our model is calibrated on Fe-poor liquids, its predictions are qualitatively in accord with such an observation, which suggests that even for basaltic magmas in non-arc settings, redox change during degassing may occur[27]. The corollary is that the iron redox state of a magma may differ significantly from that of its source, in contrast to conventional wisdom[28]. Altogether, this suggests that equating the redox state and composition of present-day volcanic gases to those emitted in the geologic past[6] may not be a correct assumption.

1. Wilson, L., Sparks, R. S. J. & Walker, G. P. L. Explosive volcanic eruptions. IV. The control of magma properties and conduit geometry on eruption column behavior. *Geophys. J. R. Astron. Soc.* **63**, 117–148 (1980).
2. Papale, P. Strain-induced magma fragmentation in explosive eruptions. *Nature* **397**, 425–428 (1999).
3. Huppert, H. E. & Woods, A. W. The role of volatiles in magma chamber dynamics. *Nature* **420**, 493–495 (2002).
4. Gonnerman, H. M. & Manga, M. Explosive volcanism may not be an inevitable consequence of magma fragmentation. *Nature* **426**, 432–435 (2003).
5. Burgisser, A. & Gardner, J. Experimental constraints on degassing and permeability in volcanic conduit flow. *Bull. Volc.* **67**, 42–56 (2005).
6. Holland, H. D. Volcanic gases, black smokers and the great oxidation event. *Geochim. Cosmochim. Acta* **66**, 3811–3826 (2002).
7. Kasting, J. F., Eggler, D. H. & Raeburn, S. P. Mantle redox evolution and the oxidation state of the atmosphere. *J. Geol.* **101**, 245–257 (1993).
8. Gerlach, T. M. Comment on paper 'Morphology and compositions of spinel in Pu'u'O'o lava (1996–1998), Kilauea volcano, Hawaii'–enigmatic discrepancies between lava and gas-based fO₂ determinations of Pu'u'O'o lava. *J. Volcanol. Geotherm. Res* **134**, 241–244 (2004).
9. Gerlach, T. M. Oxygen buffering of Kilauea volcanic gases and the oxygen fugacity of Kilauea basalt. *Geochim. Cosmochim. Acta* **57**, 795–814 (1993).
10. Roeder, P. L., Thornber, C., Proustovetov, A. & Grant, A. Morphology and composition of spinel in Pu'u'O'o lava (1996–1998), Kilauea volcano, Hawaii. *J. Volcanol. Geotherm. Res.* **123**, 245–265 (2003).
11. Moretti, R. & Papale, P. On the oxidation state and volatile behavior in multicomponent gas-melt equilibria. *Chem. Geol.* **213**, 265–280 (2004).
12. Clemente, B., Scaillet, B. & Pichavant, M. The solubility of sulphur in hydrous rhyolitic melts. *J. Petrol.* **45**, 2171–2196 (2004).
13. Gaillard, F., Schmidt, B., Mackwell, S. & McCammon, C. Rate of hydrogen–iron redox exchange in silicate melts and glasses. *Geochim. Cosmochim. Acta* **67**, 2427–2441 (2003).
14. Holloway, J. R. Thermodynamic modelling of geological materials: minerals, fluids and melts. *Rev. Mineral.* **17**, 211–233 (1987).
15. Scaillet, B. & Pichavant, M. Role of fO₂ on fluid saturation in oceanic basalt. *Nature* **430**, doi:10.1038/nature02814 (published online 28 July 2004).
16. Shi, P. F. & Saxena, F. K. Thermodynamic modeling of the C-H-O-S fluid system. *Am. Mineral.* **77**, 1038–1049 (1992).
17. Kress, V. C. & Carmichael, I. S. E. The compressibility of silicate liquids containing Fe₂O₃ and the effect of composition, temperature, oxygen fugacity and pressure on their redox states. *Contrib. Mineral. Petrol.* **108**, 82–92 (1991).
18. Wallace, P. Volatiles in subduction zone magmas: concentrations and fluxes based on melt inclusion and volcanic gas data. *J. Volcanol. Geotherm. Res.* **140**, 217–240 (2004).
19. Watson, E. B. Diffusion in volatile-bearing magmas. *Rev. Mineral.* **30**, 371–412 (1994).
20. Westrich, H. R. & Gerlach, T. M. Magmatic gas source for the stratospheric SO₂ cloud from the June 15, 1991 eruption of Mount Pinatubo. *Geology* **20**, 867–870 (1992).
21. Scaillet, B. & Pichavant, M. Experimental constraints on volatile abundances in arc magmas and their implications for degassing processes. *Spec. Publ. Geol. Soc. (Lond.)* **213**, 23–52 (2003).
22. Scaillet, B., Luhr, J. & Carroll, M. R. in *Volcanism and the Earth's Atmosphere* (eds Robock, A. & Oppenheimer, C.) 11–40 (Geophys. Monogr. 139, American Geophysical Union, Washington DC, 2003).
23. Wallace, P., Anderson, A. T. & Davis, A. M. Quantification of pre-eruptive exsolved gas contents in silicic magmas. *Nature* **377**, 612–616 (1995).
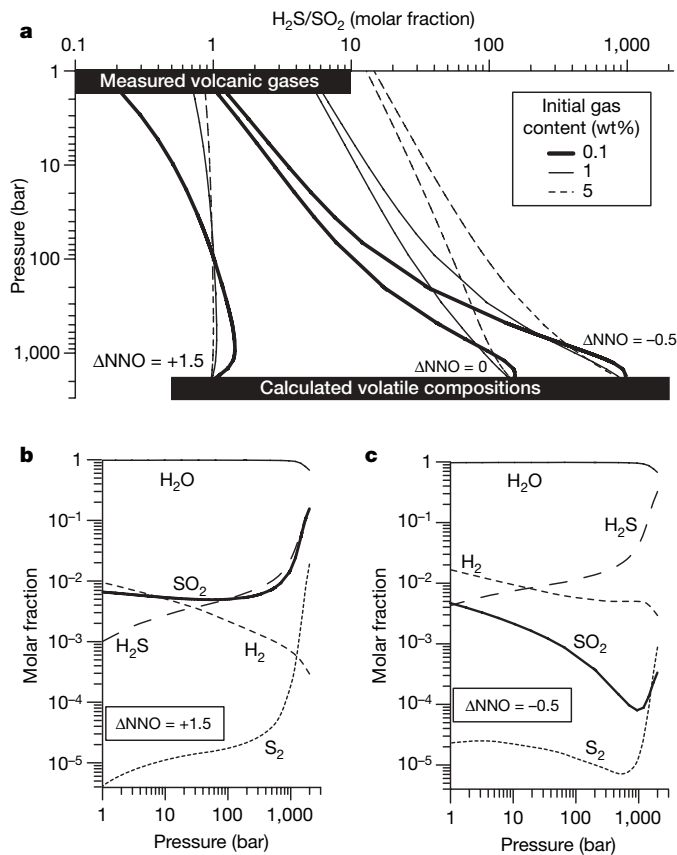
Figure 3 | Evolution of the composition of an H–O–S gas during ascent of a rhyolite magma. a, Effect of the initial redox state on the ratio H_2S/SO_2 for three starting values of f_{O_2}, each with three different gas contents (same initial conditions as in Fig. 2). Also shown are the natural range observed on active volcanoes in convergent settings[26], and the range calculated by phase equilibria experiments[21]. **b,** Evolution of the gas composition for a magma oxidized at depth (ΔNNO = +1.5, 0.1 wt% gas). **c,** Evolution of the gas composition for a magma reduced at depth (ΔNNO = −0.5, 0.1 wt% gas). Contents of O_2 are too low (<10 p.p.m.) to be displayed.

24. Gardner, J. E., Hilton, M. & Carroll, M. R. Bubble growth in highly viscous silicate melts during continuous decompression from high pressure. *Geochim. Cosmochim. Acta* **64,** 1473–1483 (2000).

25. Eichelberger, J. C., Carrigan, C. R., Westrich, H. R. & Price, R. H. Non explosive silicic volcanism. *Nature* **323,** 598–602 (1986).

26. Symonds, R. B., Rose, W. I., Bluth, G. J. S. & Gerlach, T. M. Volcanic-gas studies: methods, results, and applications. *Rev. Mineral.* **30,** 1–66 (1994).

27. Mathez, E. A. Influence of degassing on oxidation states of basaltic magmas. *Nature* **310,** 371–375 (1984).

28. Carmichael, I. S. E. The redox states of basic and silicic magmas: a reflexion of their source regions. *Contrib. Mineral. Petrol.* **106,** 129–141 (1991).

29. Holtz, F., Behrens, H., Dingwell, D. B. & Johannes, W. H$_2$O solubility in haplogranitic melts: compositional, pressure and temperature dependence. *Am. Mineral.* **80,** 94–108 (1995).

Author Contributions A.B. incorporated the thermodynamic code of gas–melt equilibria developed by B.S. into his one-dimensional conduit flow model. A.B. performed all the simulations. Both authors contributed equally to the interpretation of the model results and to the writing of the paper.

Author Information Reprints and permissions information is available at www.nature.com/reprints. The authors declare no competing financial interests. Correspondence and requests for materials should be addressed to A.B. (burgisse@cnrs-orleans.fr).

A coupled chemical-physical model of magma ascent allowed us to establish the relationship between the ascent of magma and its redox state. The chemistry formulation is based on that of Clemente et al. (2004), whereas the physical part is based on Burgisser and Gardner (2005). The gas phase is composed of n species, each with a molar fraction m_i:

$$\sum_{i=1}^{n} m_i = 1 \tag{1}$$

Conversion between molar fraction and weight fraction is:

$$x_i = \frac{m_i M_i}{\sum_j m_j M_j} \tag{2}$$

where M_i are molecular weights of each species. The total weight fraction of each species (w_{Ti}) is the sum of its exsolved part and its dissolved part:

$$w_{Ti} = w_{gT} x_i + a_i \left(f_i \right)^{b_i} \tag{3}$$

where w_{gT} is total gas weight fraction, a_i and b_i are solubility constants determined experimentally (Table 1), and f_i is species fugacity. We assume the gas phase is an ideal mixture of non-ideal gases, which yields the following expression for fugacities:

$$f_i = \gamma_i m_i P \tag{4}$$

where P is total pressure, and coefficients γ_i are calculated at each pressure step following Shi and Saxena (1992). Using (2) and (4), (3) can be written as:

$$w_{Ti} = w_{gT} \frac{m_i M_i}{\sum m_j M_j} + a_i \left(\gamma_i m_i P \right)^{b_i} \tag{5}$$

System H-O

The gas phase is composed of 3 species (H_2O, H_2, and O_2) that are in equilibrium at all times:

$$K_1 = \left(fH_2O \right)\left(fH_2 \right)^{-1}\left(fO_2 \right)^{-1/2} \tag{6}$$

where K_1 is an equilibrium constant calculated according to Robie et al. (1979). Replacing the fugacities by their expressions in (4) yields:

$$K_1 = \left(\gamma_{H2O} m_{H2O} \right)\left(\gamma_{H2} m_{H2} \right)^{-1}\left(\gamma_{O2} m_{O2} P \right)^{-1/2} \tag{7}$$

Initially, w_{gT} and fH_2 are set at a given pressure and temperature at depth. The molar composition of the gas phase can be determined by using (4) to calculate m_{H2}, (1) and (7) to calculate m_{O2}, and (1) to calculate m_{H2O}. When decompression occurs, mass conservation requires that total amounts of oxygen and hydrogen of the system remain constant. Total weight percents of atomic oxygen (w_{TO}) and atomic hydrogen (w_{TH}) can be determined from initial gas composition by using:

$$w_{TO} = M_O \left(\frac{w_{TH2O}}{M_{H2O}} + 2 \frac{W_{TO2}}{M_{O2}} \right) \tag{8a}$$

Burgisser, A., Scaillet, B. *Redox evolution of a degassing magma rising to the surface*

$$w_{TH} = M_H \left(2 \frac{w_{TH2O}}{M_{H2O}} + 2 \frac{W_{TH2}}{M_{H2}} \right) \tag{8b}$$

and replacing the total amount of each species w_{Ti} in (8) by their expressions in (5):

$$\frac{w_{TO}}{M_O} = \frac{w_{gT} m_{H2O}}{\sum m_j M_j} + \frac{a_{H2O} \left(\gamma_{H2O} m_{H2O} P \right)^{p_{H2O}}}{M_{H2O}} + 2 \frac{w_{gT} m_{O2}}{\sum m_j M_j} \tag{9a}$$

$$\frac{w_{TH}}{2 M_H} = \frac{w_{gT} m_{H2O}}{\sum m_j M_j} + \frac{a_{H2O} \left(\gamma_{H2O} m_{H2O} P \right)^{p_{H2O}}}{M_{H2O}} + \frac{w_{gT} m_{H2}}{\sum m_j M_j} + \frac{a_{H2} \left(\gamma_{H2} m_{H2} P \right)^{p_{H2}}}{M_{H2}} \tag{9b}$$

When total pressure decreases, the molar fractions (m_{H2O}, m_{H2}, and m_{O2}) and the total amount of volatiles exsolved (w_{gT}) are constrained by mass conservation, chemical equilibrium, and solubility laws embedded in the four equations (1), (7), (9a), and (9b). Using (1) and (7), m_{H2O} and m_{H2} can be expressed as a function of m_{O2}:

$$m_{H2O} = \left(1 - m_{O2} \right) \left(1 + \frac{\gamma_{H2O}}{K_1 \gamma_{H2} \sqrt{m_{O2} \gamma_{O2} P}} \right)^{-1}$$

$$m_{H2} = 1 - m_{O2} - m_{H2O} \tag{10}$$

Combining (9a) and (9b) as to eliminate w_{gT} and using (10) yields an expression for m_{O2} that we solved with an iterative procedure to find its roots:

$$\frac{w_{TH}}{2 M_H (1 - m_{O2})} - \frac{w_{TO}}{M_O (m_{H2O} + 2 m_{O2})} =$$

$$\frac{a_{H2} \left(\gamma_{H2} m_{H2} P \right)^{p_{H2}}}{M_{H2} (1 - m_{O2})} + \frac{a_{H2O} \left(\gamma_{H2O} m_{H2O} P \right)^{p_{H2O}}}{M_{H2O}} \left(\frac{1}{1 - m_{O2}} - \frac{1}{m_{H2O} + 2 m_{O2}} \right) \tag{11}$$

Because m_{H2O} is on the order of 10^{-1} and m_{O2} is usually $<10^{-10}$, it is essential to carry all calculations with sufficient numerical precision. We used a precision of 20 digits, which ensured that errors on m_{O2} values were $<0.1\%$ when $m_{O2} > 10^{-17}$.

System H-O-S

The gas phase is composed of 6 species (H_2O, H_2, O_2, S_2, H_2S and SO_2) that are in equilibrium at all times:

$$K_1 = \left(fH_2O \right) \left(fH_2 \right)^{-1} \left(fO_2 \right)^{-1/2}$$

$$K_2 = \left(fSO_2 \right) \left(fS_2 \right)^{-1/2} \left(fO_2 \right)^{-1}$$

$$K_3 = \left(fH_2S \right) \left(fO_2 \right)^{1/2} \left(fS_2 \right)^{-1/2} \left(fH_2O \right)^{-1} \tag{12}$$

where K_1, K_2, and K_3 are equilibrium constants (Ohmoto and Kerrick, 1977; Robie et al., 1979). The total weight percents of atomic oxygen (w_{TO}), atomic hydrogen (w_{TH}), and atomic sulfur (w_{TS}) are given by:

$$w_{TO} = M_O \left(\frac{w_{TH2O}}{M_{H2O}} + 2 \frac{w_{TO2}}{M_{O2}} + 2 \frac{w_{TSO2}}{M_{SO2}} \right)$$

Burgisser, A., Scaillet, B. *Redox evolution of a degassing magma rising to the surface*

$$w_{TH} = M_H \left(2 \frac{w_{TH2O}}{M_{H2O}} + 2 \frac{w_{TH2}}{M_{H2}} + 2 \frac{w_{TH2S}}{M_{H2S}} \right)$$

$$w_{TS} = M_S \left(2 \frac{w_{TS2}}{M_{S2}} + \frac{w_{TH2S}}{M_{H2S}} + \frac{w_{TSO2}}{M_{SO2}} \right) \tag{13}$$

Like the H-O system, the resolution is carried out in two steps. First, w_{gT}, fH_2O and fH_2 are set at depth so that the composition of the gas phase and the total amounts of each element could be determined. Second, each time pressure decreases, mass conservation (1) and (13), chemical equilibrium (12), and solubility laws (5) are used jointly to solve for the seven unknowns (molar fractions m_i and the total gas weight fraction w_{gT}).

Effects of Iron

When there is iron dissolved in the melt, the following redox reaction occurs:

$$2FeO + \frac{1}{2}O_2 = Fe_2O_3 \tag{14}$$

It is possible to simulate such an effect by using an empirical model that links, at constant temperature, the molar ratio of FeO and Fe_2O_3 to the oxygen fugacity (Kress and Carmichael, 1991):

$$\ln\left(\frac{m_{Fe2O3}}{m_{FeO}} \right) = a_{KC} \ln(fO_2) + \frac{b_{KC}}{T} + c_{KC} + \sum_k d_{KCk} m_k + f_{KC} \frac{P}{T} + h_{KC} \frac{P^2}{T} \tag{15}$$

where k is one of (FeO*, Al_2O_3, CaO, Na_2O, and K_2O), m_k is the total molar fraction of these species, and a_{KC}, b_{KC}, c_{KC}, $d_{KC\,k}$, f_{KC}, h_{KC} are constants given in Kress and Carmichael (1991). We calculated the redox effect of iron in the H-O-S system by using (15) and keeping track of the total amounts of Fe (w_{TFe}), oxygen in the FeO and Fe_2O_3 form ($w_{TO(Fe)}$), and oxygen in the O_2, H_2O, and SO_2 form (w_{TO}).

Because the relation (14) contains the total molar fraction of several oxides and our mass balance (13) is in weight fraction, conversions between the two units are needed, and the total composition of the melt should be known. Thus, we fixed the total weight fraction of 9 major oxides of a typical rhyolite (in wt%: SiO_2=77.44, Al_2O_3=12.88, TiO_2=0.07, CaO=0.6, Na_2O=4.14, K_2O=4.76, MgO=0.03, MnO=0.05, P_2O_5=0.03). These initial values add up to 100%, and need to be corrected to take in account the amounts of volatiles and iron. For each run, initial quantities of FeO* (w_{TFeO*}), w_{gT}, fH_2O and fH_2 are set at depth. Using the same procedure as described in "H-O-S system", total amounts of sulphur, hydrogen, and oxygen in the O_2, H_2O, and SO_2 form can be calculated. The initial amount of oxygen in the FeO and Fe_2O_3 form is not known and should be determined using the empirical equation (14). Thus, the initial quantities of the 9 major oxides are normalized so that the 9 oxides, plus the volatiles species (w_{TO}, w_{TS}, w_{TH}), plus the total iron (w_{TFeO*}) add up to 100%. Then the total molar fraction of FeO*, Al_2O_3, CaO, Na_2O, and K_2O are calculated using:

$$m_i = \frac{w_{Ti}}{M_i} \frac{1}{\sum_j \frac{w_{Tj}}{M_j}} \tag{16}$$

The total amounts of iron and oxygen fixed by the iron can be expressed as:

Burgisser, A., Scaillet, B. *Redox evolution of a degassing magma rising to the surface*

$$m_{Fe} = m_{FeO} + 2m_{Fe2O3} \tag{17a}$$

$$m_{O(Fe)} = m_{FeO} + 3m_{Fe2O3} \tag{17b}$$

From (15), we define that

$$\frac{m_{Fe2O3}}{m_{FeO}} = KC \tag{18}$$

Combining (17)-(18), we get:

$$m_{O(Fe)} = m_{Fe}\frac{1+3KC}{1+2KC} \tag{19}$$

Using $w_{TFe} = \frac{w_{TFeO*}}{M_{FeO}}M_{Fe}$ and the conversion (16) for w_{TFe} and $w_{TO(Fe)}$ yields the total amount of oxygen fixed by the iron:

$$w_{TO(Fe)} = M_O\frac{w_{TFe}}{M_{Fe}}\frac{1+3KC}{1+2KC} \tag{20}$$

The mass balance can now be rigorously carried out by adding the 9 oxides, the volatiles species (w_{TO}, w_{TS}, and w_{TH}), the total iron (w_{TFe}) and the oxygen fixed by the iron ($w_{TO(Fe)}$). The total molar fractions m_k can be updated using (16) and are used in (15) for the rest of the simulation. Because the system is closed, all the quantities involved in the mass balance, except w_{TO} and $w_{TO(Fe)}$, are considered constant. The reaction (14) imposes an exchange of oxygen between that locked in the Fe-bearing species and that involved in the H-O-S redox reactions. The sum $w_{TO} + w_{TO(Fe)} = w_{TO(Total)}$, however, remains constant. Thus, using (20), the total amount of "free" oxygen w_{TO} can be related to fO_2:

$$w_{TO} = w_{TO(Total)} - \frac{m_{Fe}M_O}{\sum_j m_j M_j}\frac{1+3KC}{1+2KC} \tag{21}$$

The numerical resolution of (21) needs to be coupled with that of the H-O-S system. For each pressure step, solving for the redox equilibrium of the volatile species (equations (1), (5), (12) and (13)) yields an fO_2. This fugacity is used in (21) to obtain a new amount of "free" oxygen. The redox equilibrium of the volatile species is solved again with the updated w_{TO}, and the process is conducted iteratively until desired precision (<10^{-5} % on w_{TO}) is reached. An under-relaxation factor of 0.1 is applied to the updated w_{TO} to ensure convergence in 20 to 30 iterations.

Runs with 1 wt% of total iron under typical storage conditions of arc rhyolites (fO_2 between NNO-0.5 and NNO+1.5) show that the buffering capacity of iron is limited to less than 0.2 unit log compared to the S-O-H system when little gas is present in the reservoir, and becomes insignificant when more gas is present in the reservoir (Fig. SI-1). Under such storage conditions, iron does not change the redox evolution of the magma with pressure. Similarly, the H_2S/SO_2 ratio changes by less than 0.2 log units when little gas is present in the reservoir and is unaffected by iron when the reservoir hosts a large amount of gas. Simulations performed with 3 wt% total iron show that the dampening effect of iron on redox change reaches 0.3-0.4 log unit with 0.1 wt% gas but only 0.3 log unit with 5 wt% gas. Beyond this iron content,

Burgisser, A., Scaillet, B. *Redox evolution of a degassing magma rising to the surface*

it is not yet possible to simulate the redox evolution owing to the lack of thermodynamic model of sulphur solubility in hydrous and Fe-rich magmas.
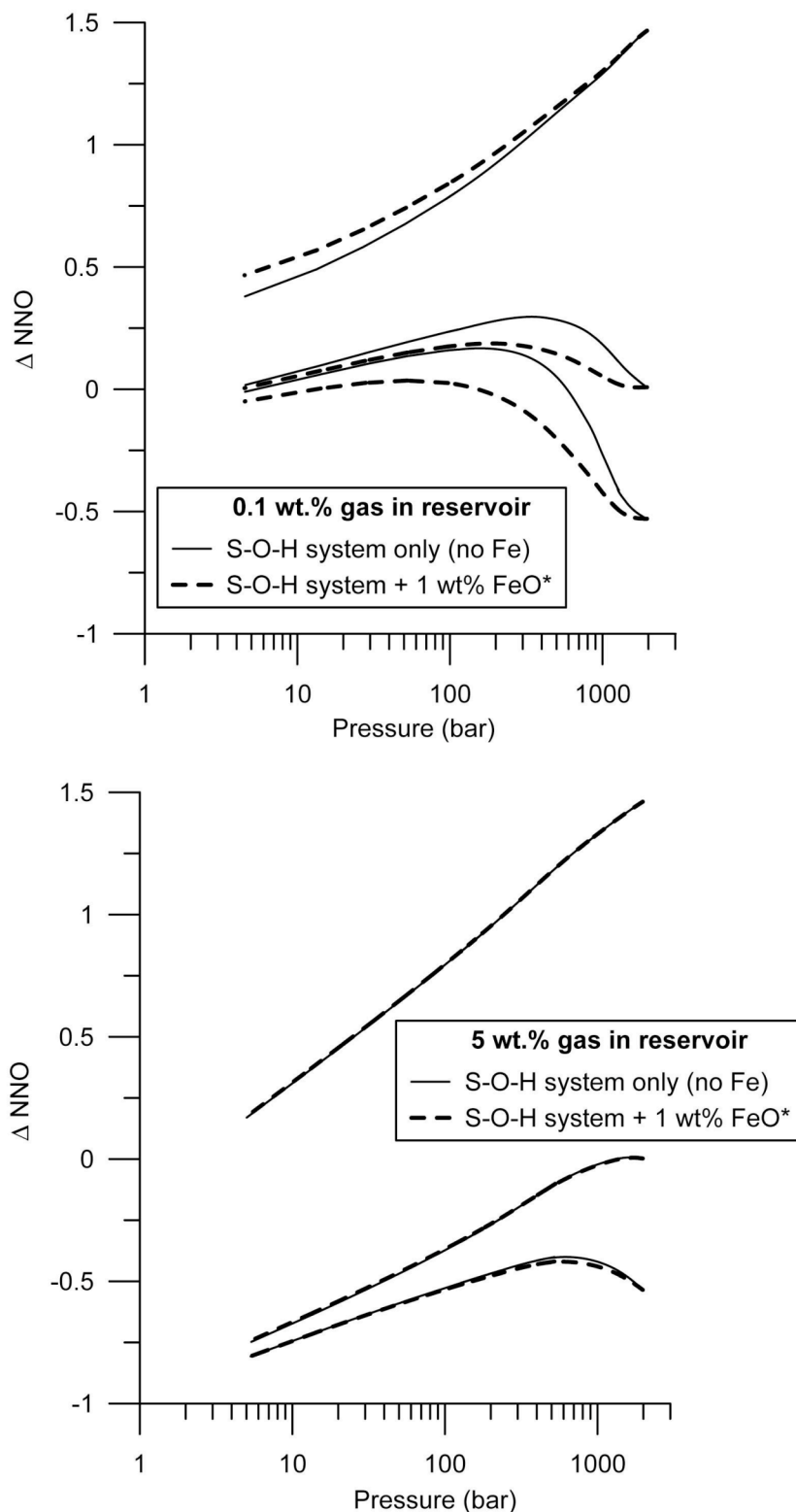

Figure SI-1: Effect of dissolved iron on the redox evolution of an ascending rhyolite. Stippled lines are runs with 1 wt.% total iron (FeO*) and solid lines are runs with no iron. Upper graph runs start with 0.1 wt.% gas at depth and lower graph runs start with 5 wt% gas at depth.

Burgisser, A., Scaillet, B. *Redox evolution of a degassing magma rising to the surface*

Physical part of the model

The conduit flow model is homogenous and one-dimensional. From mass and momentum conservation, the pressure evolution with depth (dP/dz) is given by:

$$\frac{dP}{dz} = v^2 \frac{d\rho}{dz} - \rho g - \frac{8\mu v}{r^2} - \frac{0.0025}{r} \rho v^2 \qquad (22)$$

where v is magma velocity, ρ is magma density, r is conduit radius, and g is gravity. The viscosity μ is calculated with the relationship by Hess and Dingwell (1996) for the melt and correcting for the effect of bubbles using the relationship by Dobran (1992). We note that using instead the relationship by Jaupart and Allègre (1991) for the effect of bubbles on viscosity did not change the trends caused by variations in volatile chemistry. Magma bulk density is:

$$\frac{1}{\rho} = \frac{w_{gT}}{\rho_g} + \frac{1 - w_{gT}}{\rho_l} \qquad (23)$$

where ρ_g is gas density from perfect gas law, and ρ_l is melt density. Replacing the derivative of (23) into (22) and rearranging gives:

$$\frac{dP}{dz} = \left[A\left(\frac{w_{gT}}{M} \frac{dM}{dz} - \left(1 - \frac{\rho_g}{\rho_l}\right) \frac{dw_{gT}}{dz} \right) - \rho g - \frac{8\mu v}{r^2} - \frac{0.0025}{r} \rho v^2 \right] \left[1 - \frac{A w_{gT}}{P} \right]^{-1} \qquad (24)$$

with

$$A = v^2 \rho_g \left(w_{gT} + \left(1 - w_{gT}\right) \frac{\rho_g}{\rho_l} \right)^{-2}$$

where M is the average molar mass of the gas phase:

$$M = \sum_{i=1}^{n} x_i M_i \qquad (25)$$

Above fragmentation (gas volume fraction >0.75), the viscosity is that of a dusty gas (Dobran, 1992), and degassing continues.

Equation (24) is solved using a fourth-order Runge-Kutta algorithm with adjustable distance step. At each pressure step, the gas composition is calculated for the system considered (H-O or H-O-S). The terms dM/dz and dw_{gT}/dz in (24) are evaluated implicitly, which can be justified by the fact that they are always several orders of magnitude smaller than inertia and viscous terms. Boundary condition is either atmospheric pressure at the vent, or initial velocity at depth. In the former case, a run starts with an initial guess for the velocity at depth, and the pressure is solved for until vent is reached. Initial velocity is then changed until upper boundary condition is satisfied. Because degassing occurs in equilibrium, changes in chemistry as a function of pressure are identical for the two cases.

References

Burgisser, A., and Gardner, J.E. (2005) Experimental constraints on degassing and permeability in volcanic conduit flow, Bulletin of Volcanology, v.67, p. 42-56.

Clemente, B., Scaillet, B. & Pichavant, M. The solubility of sulphur in hydrous rhyolitic melts. *J. Petrol.* 45, 2171-2196 (2004).

Burgisser, A., Scaillet, B. *Redox evolution of a degassing magma rising to the surface*

Dobran, F. (1992) Nonequilibrium flow in volcanic conduits and application to the eruptions of Mt. St. Helens on May, 18, 1980, and Vesuvius in AD 79, Journal of Volcanology and Geothermal Research, v.49, p. 285-311.

Hess, K-U., and Dingwell, D.B. (1996) Viscosities of hydrous leucogranitic melts: A non-Arrhenian model, American Mineralogist, v.81, p. 1297-1300.

Jaupart C, and Allègre C (1991) Gas content, eruption rate and instabilities of eruption regime in silicic volcanoes, Earth Planet Sci Lett 102:413-429

Kress, V.C., and Carmichael, I.S.E. (1991) The compressibility of silicate liquids containing Fe_2O_3 and the effect of composition, temperature, oxygen fugacity and pressure on their redox states, Contributions to Mineralogy and Petrology, v.108, p. 82-92.

Ohmoto, H., and Kerrick, D.M. (1977) Devolatilisation equilibria in graphitic systems, American Journal of Science, v.277, p. 1013-1044.

Robie, R.A., Hemingway, B.S., and Fisher, J.R. (1979) Thermodynamic properties of minerals and related substances at 298.15 K and 1 bar (10^5 Pa) pressure and at higher temperatures, US Geological Survey Bulletin 1452.

Shi, P.F. & Saxena, F.K. (1992) Thermodynamic modeling of the C-H-O-S fluid system. Amer. Mineral. 77, 1038-1049.

Burgisser, A., Scaillet, B. *Redox evolution of a degassing magma rising to the surface*